Electrochimica Acta 110 (2013) 809–815

Contents lists available at ScienceDirect

Electrochimica Acta

journal homepage: www.elsevier.com/locate/electacta

# Solids at the liquid–liquid interface: Electrocatalysis with pre-formed nanoparticles

Yvonne Gründer[a], Marcel D. Fabian[a,1], Samuel G. Booth[a], Daniela Plana[b], David J. Fermín[b], Patrick I. Hill[c], Robert A.W. Dryfe[a,*]

[a] School of Chemistry, University of Manchester, Oxford Road, Manchester M13 9PL, UK
[b] School of Chemistry, University of Bristol, Cantock's Close, Bristol BS8 1TS, UK
[c] School of Chemical Engineering & Analytical Science, University of Manchester, Oxford Road, Manchester M13 9PL, UK

ARTICLE INFO

*Article history:*
Received 5 December 2012
Received in revised form 25 March 2013
Accepted 27 March 2013
Available online 8 April 2013

*Keywords:*
Liquid–liquid electrochemistry
Electrocatalysis
Nanoparticles

ABSTRACT

The catalytic activity of Au and Au–Pd core–shell nanoparticles is investigated at the liquid–liquid interface. The particles are shown to catalyse a process which is attributed to interfacial oxygen reduction. The Au–Pd particles are shown to be more active and correlations made between the catalytic activity and particle radius, surface area and concentration give insight into the mechanism of the catalytic process. Comparison is also made with an analogous bipolar configuration, formed by making contact between the liquid half-cells using a gold wire.



## 1. Introduction

Electrochemistry at the interface between two immiscible electrolyte solutions (ITIES) has become an important sub-domain of electrochemistry. Ion transfer, assisted ion transfer and electron transfer are possible and more complex reactions can occur at the interface, which involve coupled ion and electron transfer. Recently there has been considerable interest in the catalysis of reactions, such as the oxygen reduction reaction (ORR) or hydrogen evolution reaction (HER), at the liquid–liquid interface. Catalysis can be achieved through adsorption of larger molecules [1–4], through the growth of metallic deposits [5,6] or through the adsorption of solid catalysts ($MoS_2$) [7,8].

The HER at the liquid–liquid interface without any catalyst present [9] and its catalysis through the adsorption of molybdenum disulfide has been investigated [7] under anaerobic conditions. The mechanism proposed is a proton-coupled electron transfer (PCET). The proton is transferred from the aqueous phase to the organic phase upon which it is reduced to hydrogen in the organic phase. The possible reactions involving protons and oxygen are summarised in Table 1 together with the corresponding standard potentials in an aqueous phase at pH 3, in 1,2-dichloroethane (DCE) and in 1,2-dichlorobenzene (DCB). As can be seen from this table, the standard reduction potentials are more positive in the organic phase, therefore with ferrocene derivatives ($E_0$ in the range 0.03–0.57 V vs. SHE) [10] as reducing agents these reactions can occur spontaneously in the organic solution.

In the presence of oxygen the proton transfer is followed by a two-electron oxygen reduction reaction to hydrogen peroxide and/or by a four-electron oxygen reduction reaction to water [11,12]. The catalysis of this reaction using porphyrin molecules has been investigated at the water|DCE [1,3,4,13] and the water|DCB [10] interfaces.

The modification of the liquid–liquid interface is also possible through adsorption of metallic nanomaterials. The assembly of gold nanoparticles at the liquid–liquid interface can be probed by optical methods which are very sensitive to the surface plasmon resonance of the gold particles as was shown experimentally [14] and theoretically [15]. Similarly, the influence of a film of nanoparticles adsorbed at the liquid–liquid interface on the interfacial capacitance was investigated experimentally [16] and theoretically [17]. It was further shown that an enhancement of photocurrent response can be achieved through the adsorption of gold nanoparticles at the water|DCE interface due to the plasmon resonance of the adsorbed gold [18].

Nanoparticles are widely investigated for their catalytic activity due to their high surface to bulk atom ratio and the achievable

* Corresponding author. Tel.: +44 161 306 4522; fax: +44 161 275 4598.
*E-mail address:* robert.dryfe@manchester.ac.uk (R.A.W. Dryfe).
[1] Present address: Department of Pure & Applied Chemistry, Carl von Ossietzky University Oldenburg, Faculty of Mathematics & Natural Sciences, D-26111 Oldenburg, Germany.

0013-4686 
http://dx.doi.org/10.1016/j.electacta.2013.03.185

**Table 1**
Electrochemical reactions involving proton reduction and the corresponding standard potentials vs. SHE in aqueous solution of pH 3, DCE and DCB are summarised.

| | $E_0$ in acidic solution (pH 3)/V | $E_0$ in DCE/V | $E_0$ in DCB/V |
|---|---|---|---|
| $O_2 + 2H^+ + 2e^- \rightarrow H_2O_2$ | 0.482 | 1.166 | 1.24 |
| $O_2 + 4H^+ + 4e^- \rightarrow 2H_2O$ | 1.051 | 1.749 | 1.86 |
| $H^+ + e^- \rightarrow ½H_2$ | −0.177 | 0.55 | 0.68 |

high surface area at low bulk concentration and associated lower cost. Studies of the reactivity of nanoparticles as catalysts for electrochemical reactions involve the adsorption or growth of nanomaterials onto solid substrates, e.g. carbon materials [19,20], oxide materials [21], metal substrates [22] or molecular templates [23], which allow formation of an electronic contact required to control electrochemical reactions. The potential is then applied through the substrate material. Although the substrate is chosen with a low activity for the specific catalysed reaction, the potential distribution at the interface and the electrochemical results might be influenced through the substrate double layer [24]. To decouple substrate–nanoparticle and substrate–electrolyte interaction from the electrochemical results is therefore not straightforward. The effect of gold particles supported on a solid substrate on the catalysis of the ORR has been widely investigated and a higher activity towards the 4-electron step reaction has been found for smaller particles [20,22,25]. It is, however, difficult to decouple the effect of particle coverage, active surface area and surface geometry unambiguously from the observed changes in the rate constants [25]. The liquid–liquid interface enables the electrochemical properties of nanoparticles to be probed without having to consider the influence from a solid substrate and is a promising tool to combine electrochemical (particularly electrocatalytic) reactions at solid surfaces with the advantage of having two solvents to transport reacting species. Specifically, the adsorption of crystalline nanomaterials at the ITIES is a promising way to combine solid–liquid electrocatalysis with the advantage of the liquid–liquid interface (e.g. higher solubility of oxygen in organic solvents).

In this paper we present a new approach to study the electrocatalytic activity of nanomaterials for ORR through adsorption at the liquid–liquid interface. This setup allows the direct probing as the nature and amount of the adsorbed particles is easily varied. In addition, the bipolar setup, in which the two liquid phases are separated in two half-cells without forming a liquid–liquid interface, only connected by a conducting material [26], allows the direct comparison of the response with that of the corresponding bulk material at the liquid–liquid interface and therefore resolves any contribution due to ion transfer in the net catalytic process.

The effect of adsorption of (i) gold nanoparticles of different size and of (ii) Pd shell–Au core nanoparticles with fixed core size, but varying shell thickness, is reported here.

## 2. Experimental

Glassware was cleaned in a 1:4 mixture (by volume) of Piranha solution (30% hydrogen peroxide, $H_2O_2$, and concentrated sulphuric acid, $H_2SO_4$, Fisher Scientific), boiled in ultra-pure water and dried. Solutions for the aqueous phase were prepared using ultra-pure water (18.2 MΩ cm). LiCl (99.99%, Aldrich) was used as the aqueous base electrolyte at a concentration of 0.1 M. Hydrochloric acid (99.999%, Sigma–Aldrich) was used to adjust the pH to 3. 1,1′-Dimethylferrocene (DiMFc, 97%, Alfa Aesar) was used as the reducing agent in the organic phase. The organic solvent was DCB (≥99%, supplied by Fluka). The organic phase electrolyte bis(triphenylphosphoranylidene)-tetrakis[3,5-bis(trifluoromethyl) phenyl] borate (BTPPATPBF) was prepared as described elsewhere [1] from sodium tetrakis[3,5-bis (trifluoromethyl)phenyl]borate (97%, Alfa Aesar) and bis(triphenylphosphoranylidene)ammonium chloride (97%, Sigma).

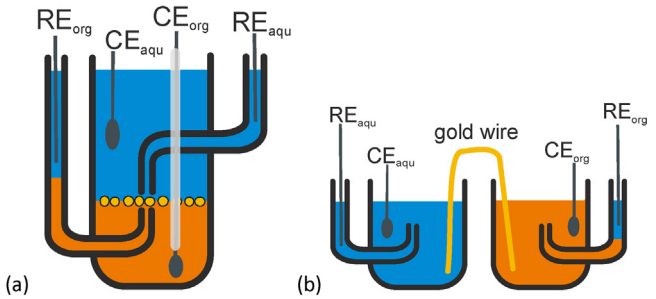


**Fig. 1.** The four electrode electrochemical cells employed for (a) liquid–liquid electrochemistry experiments and for (b) bipolar experiments.

The gold nanoparticles (5, 14 and 19 nm in diameter) were synthesised from aqueous solutions of $HAuCl_4$, following well established colloidal methods, using sodium citrate as reducing agent and stabiliser; in order to obtain the smallest diameters (5 nm), tannic acid was added as a stronger ligand [27–29]. The Au–Pd core–shell particles were produced using the as-prepared 19 nm Au particles as cores; varying amounts of $H_2PdCl_4$ were reduced to form the Pd shells over the Au cores, using L-ascorbic acid as reducing agent [28,30,31]. The resulting core–shell particles are stabilised by both citrate and ascorbic acid. As expected from the synthesis conditions used, and confirmed by TEM and EDX measurements, the Pd20Au80 nanoparticles are 20 wt.% Pd and 80 wt.% Au, with an average shell of 1.1 nm; the Pd80Au20 on the other hand have the opposite weight ratio and an average Pd shell thickness of 9 nm.

Cyclic voltammetry experiments were performed using a four electrode configuration (Fig. 1) with an Autolab potentiostat (PGSTAT100). Homemade Ag/AgCl reference electrodes (RE) were directly immersed in the chloride containing aqueous phase. An aqueous solution of 0.1 mM LiCl and 1 mM BTPPACl (bis(triphenylphosphoranylidene) ammonium chloride) was brought in contact with the organic solution and formed a liquid junction for the organic reference electrode. The organic counter electrode was glass coated to avoid contact of the Pt with the aqueous (upper) phase. The cells used for the liquid|liquid electrochemical measurements at the water|DCB interface, had a cross-sectional area in the range 0.63–0.78 $cm^2$ and a total solution volume of 3 ml. A schematic of such a cell is shown in Fig. 1a. The cells used for the bipolar setups had a solution volume of about 1.5 ml in each phase and were connected through a 0.5 mm diameter gold wire annealed in a butane flame until glowing red prior to experiment. The resulting electrochemical cell is summarised in Fig. 1b.

To prepare samples for the transmission electron microscopy (TEM), a drop of 10 μl colloidal solution was deposited on holey 300 copper mesh grids covered with a holey carbon film (Agar scientific). When the solution was evaporated the samples were imaged using an FEI Tecnai F30 transmission electron microscope operating at 300 kV. Bright field imaging mode was used and images recorded digitally.

## 3. Results and discussion

### 3.1. Transmission electron microscopy (TEM)

The gold nanoparticles of 5 nm and 19 nm diameter, and the Pd80Au20 particles, were characterised by TEM. The resultant

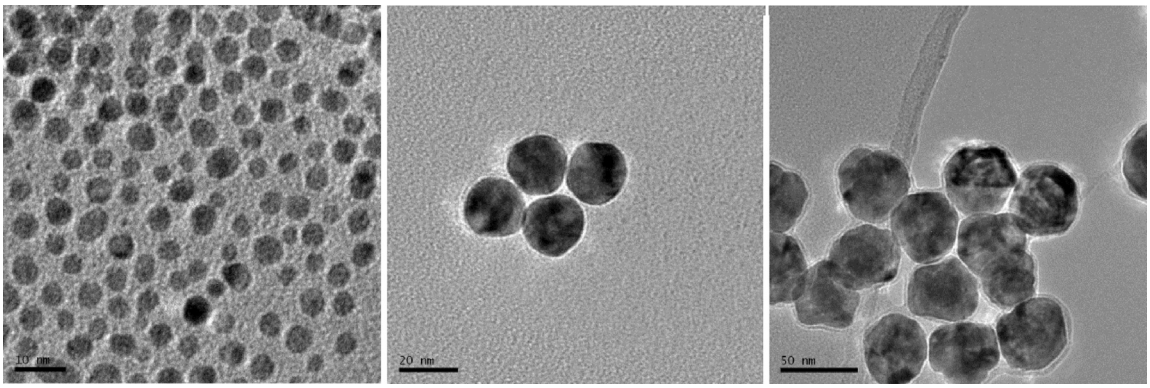


**Fig. 2.** TEM image of gold (5 nm) particles, gold (19 nm) particles and Pd80Au20 particles. The scale bars, from left to right, are 10 nm, 20 nm and 50 nm.

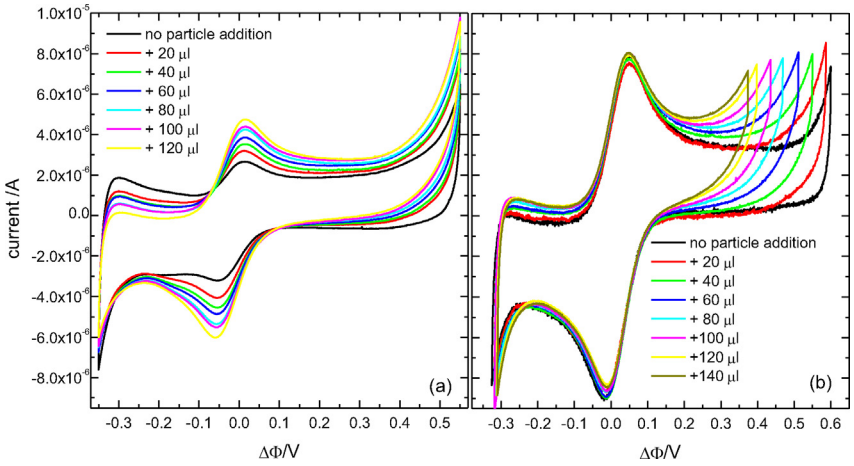


**Fig. 3.** Cyclic voltammograms obtained with the cell described in Scheme 1 upon addition of successive addition of 20 µl of (a) colloidal solution of Pd shell gold core nanoparticles with a 19 nm gold core and a 9 nm thick Pd shell and upon addition of (b) a colloidal solution of gold nanoparticles with a diameter of 14 nm. The currents at the positive limit of the potential window increase in both cases with successive additions of nanoparticles.

micrographs are shown in Fig. 2. As can be seen from the images, the particles have a uniform size distribution as expected from the preparation. The particles also tend not to agglomerate, which points to intact ligands and a stable colloidal solution. Previous detailed HRTEM studies of particles prepared under the same conditions have shown that the Pd layer is continuous over the Au core, even for the 1 nm shell. The average lattice strain of the Pd-shell relaxes by more than 2% upon increasing the shell thickness from 1 to 10 nm [28]. Very little evidence of substantial alloying has been observed under these growth conditions [28].

### 3.2. Cyclic voltammetry at the liquid–liquid interface

Electrochemical measurements at the water|DCB interface were performed using the cell shown schematically in Fig. 1a with a four-electrode configuration. The cell composition is defined in Scheme 1. DiMFc was chosen as reducing agent as its standard potential ($E_0$ = 0.573 V [10] in DCB) is high enough to allow the 2- and 4 electron oxygen reduction but low enough to exclude the interfacial HER (Table 1). Fig. 3 shows cyclic voltammograms obtained from the bare liquid–liquid interface and after successive addition of 20 µl aliquots of colloidal solution containing Pd80Au20 particles (Fig. 3a) and Au 14 nm diameter particles (Fig. 3b) injected close to the interface on the aqueous side. Prior to these measurements cyclic voltammograms at slower scan rates (20 mV/s and 10 mV/s) were recorded in the same potential range as the subsequent cyclic voltammogram recorded at 50 mV/s and presented in Fig. 3. The data presented here was recorded about 30 min after each particle addition, when no further change in the cyclic voltammogram could be observed with time. This time delay is necessary to allow each new aliquot of particles to reach the interface, although this procedure has the disadvantage of permitting spontaneous oxidation of the DiMFc reducing agent to occur (the voltammetry was recorded under ambient conditions, with no solution de-gassing). A reversible current peak can be observed at $\Delta\Phi$ = 16 mV, with $\Delta\Phi$ defined as the difference between the potential of the aqueous and the organic bulk phases, $\Delta\Phi = \Phi(w) - \Phi(o)$. This current is due to the ion transfer of the oxidised dimethylferrocene, $DiMFc^+$ [10], formed by oxidation of the neutral DiMFc initially present in the organic phase. The resultant $DiMFc^+$ ion transfer peak was used to adjust the absolute potential scale of the cyclic voltammograms. The main evolution in the voltammograms of Fig. 3a is in the positive limit of the potential window, which shifts to lower potentials with each addition of Au nanoparticles.

| | | | | |
|---|---|---|---|---|
| $Ag/AgCl_{(s)}$ | 0.1 M LiCl, 1 mM $BTPPACl_{(aq)}$ | 4 mM 1,1'-Dimethylferrocene, 15 mM $BTPPATFPB_{(DCB)}$ | 0.1 M LiCl, 1 mM $HCl_{(aq)}$ | $Ag/AgCl_{(s)}$ |

**Scheme 1.** The cell composition which was employed for the presented electrochemical experiments.

**Table 2**
Properties of the colloidal nanoparticle solutions employed for the experiments are summarised. The volume per particle, particle concentration per volume, surface area per particle and surface area per volume were determined.

| | Volume per particle ($nm^3$) | Particles ($\mu l$) | Circumference per particle (nm) | Total circumference | Surface area per particle ($nm^2$) | Surface area ($nm^2/\mu l^{-1}$) |
|---|---|---|---|---|---|---|
| Au 5 nm | 77.95 | $3.80 \times 10^{10}$ | 15.7 | $5.97 \times 10^{11}$ | 88.25 | $3.35 \times 10^{12}$ |
| Au 14 nm | 1663.9 | $1.78 \times 10^{9}$ | 44.0 | $7.83 \times 10^{10}$ | 678.9 | $1.21 \times 10^{12}$ |
| Au 19 nm | 3591.4 | $7.10 \times 10^{8}$ | 59.7 | $4.24 \times 10^{10}$ | 1134.11 | $8.06 \times 10^{11}$ |
| Pd20Au80 | 4989 | $6.02 \times 10^{8}$ | 66.6 | $4.00 \times 10^{10}$ | 1411.96 | $8.50 \times 10^{11}$ |
| Pd80Au20 | 26,521 | $3.34 \times 10^{8}$ | 116.2 | $3.88 \times 10^{10}$ | 4300.9 | $1.43 \times 10^{12}$ |

Similar cyclic voltammograms were obtained upon the subsequent addition of 20 μl of colloidal solution of Pd20Au80 particles and upon the addition of colloidal gold particles with diameters of 5 nm and 19 nm.

To quantify the current increase upon addition of colloidal nanoparticles, the double layer current of the cyclic voltammogram prior to addition was determined and the potential at which the current increased by half was noted. For the cyclic voltammograms recorded with the particles present, the potential at which this additional faradaic current was reached was determined. This procedure was necessary as the exact area of the liquid–liquid interface differs for each preparation, due to its different shape and varying diameter of the electrochemical cells employed. Without particles present the positive limit of the potential window is determined by the transfer of the $Li^+$ and protons; the Gibbs energies of transfer between aqueous phase and DCE of both species are comparable [32–34] and relate linearly to the Gibbs energies of transfer between water and DCB [10,35]. Upon addition of the particles an alternative process is activated, which narrows the potential window at the positive end. This shift in potential with respect to the bare liquid–liquid interface for each preparation is plotted in Fig. 4 for the different additions of nanoparticles per volume colloidal solution. It is clear that a larger shift in potential is observed for the Pd shell–Au core particles, compared against the pure Au particles, with a slightly bigger shift for the particles with thicker Pd shell, hence higher surface area. For the gold particles a more pronounced shift of the end of the potential window is observed for smaller particles, with the largest shift for the 5 nm diameter gold particles and the smallest for the 19 nm gold particles.

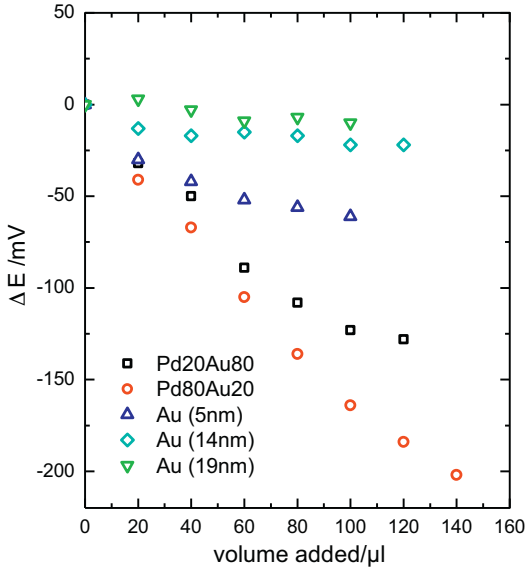


**Fig. 4.** The shift in potential of the positive end of the potential window observed for different kinds of nanoparticle per volume of colloidal solution added.

Using the diameter of the different nanoparticles, their respective circumferences, surface areas, and volumes could be obtained, assuming completely spherical particles. The $HAuCl_4$ starting concentration was $2.5 \times 10^{-4}$ M for the preparation of 19 nm particles and $2.9 \times 10^{-4}$ M for the formation of 5 and 14 nm particles. Knowing the atomic weight of gold and its density, the number of particles and their total surface area per volume of colloidal suspension could then be determined (as shown in Table 2). For the core–shell nanostructures, the concentration of particles in solution was determined from the dilution of the 19 nm Au core colloidal suspension, through the addition of the Pd salt solution and the ascorbic acid; it can be seen in Table 2 that the total metal surface area per volume of solution increases with the Pd shell thickness, despite larger dilution factors.

For the gold particles, a greater shift in the positive end of the potential window is observed with the smaller particles when analysed per volume added. Due to the similar starting concentration of gold in the synthesis of the colloidal solutions however, there is a larger number of smaller particles per unit volume and due to the greater ratio of surface to bulk atoms, the smaller particles also have a larger active metal surface area and form a larger three phase junction at the interface per unit volume. The active surface area quoted is the total surface area of the gold nanoparticles, which is the product of particles per volume and surface area per particle.

The active area responsible for the catalysing effect, however, is not straightforward to determine as the exact adsorption behaviour of the particles at the interface is not presently known and only part of the surface of each particle will be in contact with the aqueous or organic phase. Although we cannot say how much of the particles added adsorb at the interface, there is equilibrium between the number of particles in the bulk of the aqueous solution and at the liquid–liquid interface [36,37]. Citrate and mercaptosuccinic acid stabilised gold particles have been previously shown to adsorb reversibly to the liquid–liquid interface at a potential close to the negative end of the accessible window [16,36].

The potential shift due to the increasing current is shown in Fig. 5 as a function of the number of particles added (independent of the radius, $R$, of the particles), as function of the total circumference (proportional to $R$), which is a measure of amount of the total contact line created by the three phase junction of particle|organic|aqueous, and as a function of the total surface area (proportional to $R^2$). It can be seen that the potential shift depends exponentially either on the number of particles added or, more likely, on the circumference of the particles added, which is proportional to the length of the three phase junction of DCB|aqueous phase|gold particles and was obtained as the product of the number of particles and the circumference of one particle. Although the circumference of the particle at its maximum is probably not exactly co-incident with the three phase junction, and in any case is likely to change as a function of applied potential, both the circumference and the three phase junction scale linearly with $R$. This leads to the conclusion that the catalytic activity of the gold particles is not due to surface area but more likely to an effect facilitating the reaction at the three phase junction, or to a 'storage' of electrons [7] to facilitate multi-electrons reactions through the newly formed

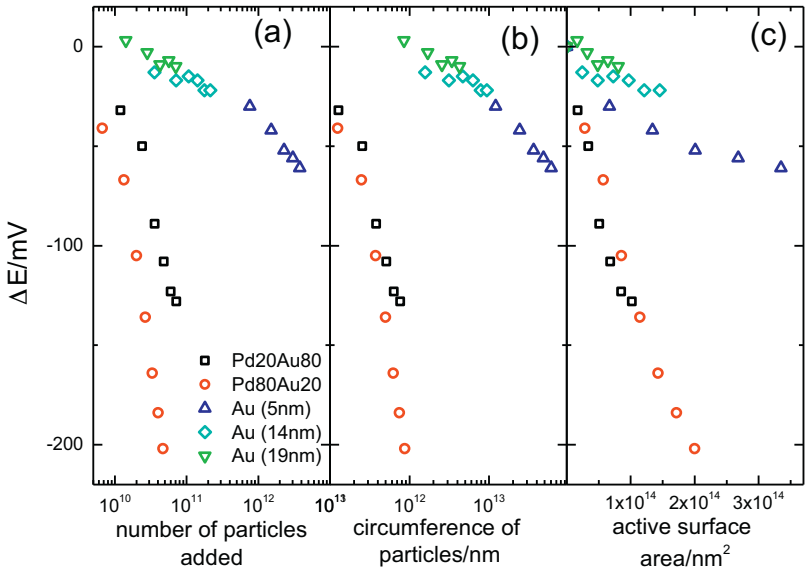


**Fig. 5.** The shift in potential of the positive end of the potential window observed for different kinds of colloidal nanoparticle solution per circumference of particles added (a), per active metal surface added (b) and per number of particles added (c).

three phase junction and the increased space available for one reaction.

The catalytic activity of the Pd shell particles is much more pronounced than for the gold particles. Conducting the same kind of normalisation of the potential shift to the number of particles added, the total length of the three phase junction and the active metal surface shows a different behaviour than for the gold particles (see Fig. 5). The Pd80Au20 particles produce a stronger shift of the onset of the current with potential per particle. As can be seen in Fig. 5c when looking at the shift per active metal area, the catalytic effect is reproduced smoothly and can therefore be attributed to the larger surface area per particle due to the bigger Pd shell.

We can conclude that the catalysing effect of the Au–Pd core–shell particles is a surface area effect, which might be due to the larger area available for hydrogen adsorption. The catalysing effect may due to proton adsorption and successive transfer to the organic phase where the proton is involved in subsequent homogeneous reduction or due to the hydrogen adsorption and consecutive heterogeneous reaction: no unambiguous selection of mechanism is possible from this data. However catalysis due to hydrogen absorption, as opposed to hydrogen adsorption, can be excluded as the shift in potential would then depend on the Pd volume rather than on the surface area, which is much larger for thicker Pd shells.

### 3.3. Cyclic voltammetry with a bipolar setup

The underlying process of the catalysing effect of materials adsorbed at the liquid–liquid interface has been, for different catalytic materials, explained through assisted proton transfer from aqueous to the organic phase and subsequent homogeneous reduction in the organic phase [2]. To verify this process for the present case, a bipolar cell (Fig. 1b) was employed in which the organic and aqueous phase are only in contact through a gold wire. This is a variant of the "electronic conductor separating the organic/water interface" (ECSOW) configuration reported by Osakai for simple electron transfer processes at the ITIES [26]. The cyclic voltammogram recorded with the same concentrations of reactants and supporting electrolyte in DCB and aqueous half-cells of the bipolar cell is shown in Fig. 6.

In addition, cyclic voltammograms were recorded at (i) the water|DCB interface where, instead of nanoparticles, an isolated gold wire (annealed in a butane flame until glowing red prior to experiment) was inserted to bridge the interface and (ii) a separate experiment where the cyclic voltammogram for a gold wire in the aqueous solution was recorded against a Ag/AgCl reference electrode (Fig. 6a and c, respectively). As for the cyclic voltammogram recorded at the liquid–liquid interface, the potential scale for the bipolar setup and for the gold wire at the liquid–liquid interface had to be corrected by the potential drop at junction of the organic reference electrode, which was determined to be −450 mV. To compare the gold wire measured in aqueous solution using the Ag/AgCl reference electrode with the liquid–liquid and bipolar cells, the Ag/AgCl potential scale had to be linked to the DiMFc potential scale (against which all reduction processes are occurring, in these liquid–liquid systems). The standard potential of $DiMFc^+$/DiMFc in DCB is 0.57 V vs. SHE [10]. The potential of the Ag/AgCl reference electrode in 0.1 M LiCl solution is 0.288 V vs. SHE, which gives a net offset of 0.282 V vs. the interfacial potential at the liquid–liquid

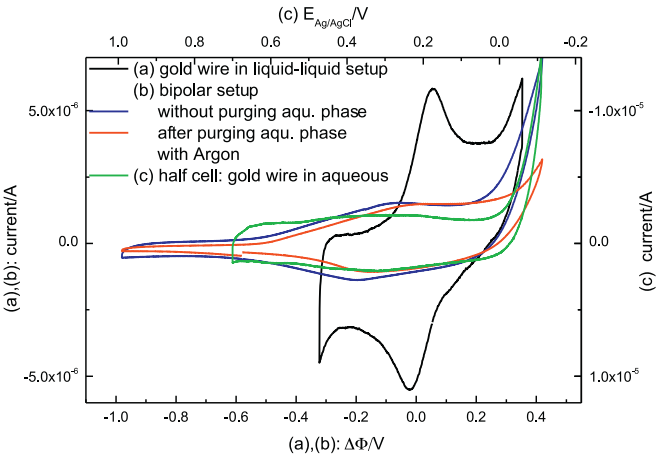


**Fig. 6.** Cyclic voltammograms for the cell composition presented in Scheme 1 for a liquid–liquid cell with a gold wire bridging the interface (a), for a bipolar setup consisting of two half cells bridged by a gold wire with and without argon purging (b), and for a gold wire in the aqueous half cell (c). (For interpretation of the references to colour in the text, the reader is referred to the web version of the article.)

interface. In addition, for the bipolar and liquid–liquid systems, positive applied potentials correspond to the aqueous phase being polarised positively and positive current refers to electron or anion transfer from the organic to the aqueous phase or, equivalently, cations being transferred from the aqueous to the organic phase [38]. For the gold wire in aqueous solution the aqueous phase was polarised negatively at positive potentials and positive current was recorded for electron transfer from the aqueous phase to the gold wire. Therefore potential and current scales for the gold wire setup in aqueous solution are reversed with respect to the liquid–liquid interface. As can be seen from this comparison, the onset of increased positive current occurs at potentials in the range $0.2\,V < \Delta\Phi < 0.3\,V$, which is about the same potential region seen in the liquid–liquid case for the maximum shift induced by the adsorbed nanoparticles. Given that this potential is too low to drive aqueous proton reduction coupled to DiMFc oxidation, and that the bipolar and three-electrode configurations exclude the possibility of proton transfer to the organic phase, we therefore conclude that the underlying mechanism of the catalytic reaction does not involve an interfacial ion transfer. In support of this, the bipolar cell was investigated for the case where the aqueous phase was purged with argon (Fig. 6(b), red trace). The extension of the positive potential limit suggests that this limit is, indeed, associated with oxygen reduction.

The onset potential of increased current in the three experimental configurations shown in Fig. 6 (the bipolar experiment, the liquid–liquid experiment with a gold wire present and the half-cell of the gold wire in aqueous solution) is more negative (0.3 V) than in the liquid–liquid cell with gold nanoparticles adsorbed at the interface (the highest shift observed for a total addition of 100 μl of colloidal solution of 5 nm diameter gold particles was 0.5 V). This indicates that the catalytic activity of the nanoparticles is actually less strong than that of the gold wire, which may be caused by a difference in the catalytic mechanism. For the gold nanoparticles a catalytic effect governed by the number of nanoparticles was found, which was associated with charge storage or increased available space for one reaction at the three phase boundary. The exact mechanism of the catalytic effect and the exact oxygen reduction reaction cannot be deduced from this data alone. We note however that for gold nanoparticles adsorbed on solid substrates [20,22,25] both ORR reactions occur, with a higher activity towards the 4-electron reaction seen for smaller particles. The dimensions of the gold wire are much larger than those of the gold nanoparticles; therefore differences in the origin of the catalytic reaction could arise from deviations in charge arrangements and potential drop at the extremities of the wire compared to the case of Au adsorbed directly at the liquid–liquid interface. We note that significant differences in the hydrogen adsorption behaviour of Au nanoparticles, compared to macroscopic Au electrodes, have been reported recently [39]. By contrast, the potential shift observed with the Pd shell–Au core nanoparticles, is comparable to the three cases noted in Fig. 6 (the bipolar setup, the Au wire in the liquid–liquid cell and the gold wire in the aqueous half-cell). We therefore conclude that the catalytic effect of the Pd shell–Au core nanoparticles is similar to the gold wire, depending on the exposed surface area.

Another factor that could reduce the catalytic activity of the gold nanoparticles is the blocking of the reaction through remaining ligands or different chloride adsorptions on the nanoparticle surface. The 14 nm gold, 19 nm gold and the Pd Au–core shell nanoparticles are stabilised by citrate whereas, the 5 nm diameter particles have a different ligand (tannic acid compared to citric acid for the bigger particles). The change in ligand identity does not seem to affect the catalytic activity of the particles as the behaviour depends smoothly on the size of the three phase junction formed by particles added to the system with the organic and aqueous phase (Fig. 5a). The potential-dependent adsorption of citrate on Au(1 1 1) electrodes has been investigated in the absence and presence of chloride [40] at pH = 6.3 and similar behaviour was observed in both cases, indicating the preferential adsorption of citrate. Kunze et al. [41] investigated the adsorption of citrate on Au(1 1 1) electrodes at pH 1 and pH 3 in absence of chloride and found a weakening in the adsorption strength with decreasing pH. The Gibbs energies of adsorption, $\Delta G_{ads}$, for citrate at pH 1 and pH 3 were determined in a potential range of 0.52–0.92 V (vs. SHE) to be in the range of 120–200 kJ mol$^{-1}$ and to increase with increasing applied potential. Again, it was concluded that citrate is slightly more strongly adsorbed than chloride, with the Gibbs energy of adsorption for chloride on Au(1 1 1) varying from 115–135 kJ mol$^{-1}$ [42] in the same potential range. The adsorbate coverage also depends on the adsorbate concentration in solution. With similar $\Delta G_{ads}$ values for chloride and citrate, and a chloride concentration of 0.1 M in the aqueous phase compared to no excess citrate, it can therefore be assumed that the nanoparticles adsorbed at the liquid–liquid interface are stripped of their original citrate ligands, either through potential cycles prior to each measurement or through replacement with ions of the supporting electrolytes.

To compare this potential range to the interfacial applied potential in the liquid–liquid phase is not straightforward: for electrochemical processes involving electron transfer the reaction is defined by the standard potential and the potential range has to be converted against the potential of the electron acceptor/donor couple in the organic phase as performed here for the bipolar cell. In our case the electron donor/acceptor is the DiMFc/DiMFc$^+$ couple and a potential range of 0.52–0.92 V (vs. SHE) corresponds to a Galvani potential difference, $\Delta\Phi$, range of −0.05 to −0.45 V (note: the inversion of the sense of the potential scales due to the aforementioned change in polarisation of the aqueous phase in the four-electrode set up). Chemisorption processes, however, are driven by the total charge at the solid electrode, e.g. anions adsorb positive of the potential of zero charge (pzc) [43,44]. The potential of zero charge of the liquid–liquid interface can be determined from an ion transfer with a known Gibbs energy of transfer; the potential scale is then given as absolute potential. The adsorption of nanoparticles at the liquid–liquid interface, however, alters the interfacial capacitance and shifts in the minimum of the capacitance of about 0.05 V have been observed upon adsorption of citrate covered gold nanoparticles. On Au(1 1 1) the pzc is about 0.45 V (vs. SHE). By comparing this value to the pzc of the liquid–liquid interface, the potential range of 0.52–0.92 V (vs. SHE) on a gold electrode corresponds to a $\Delta\Phi$ range of −0.07 V to −0.47 V, which is on the same order as the potential scale adjustment with respect to the DiMFc/DiMFc$^+$ couple. The onset of current due to the catalysed ORR is observed positive of the pzc, in a potential region where no citrate or chloride should be adsorbed on gold in the aqueous phase.

## 4. Conclusions

In this paper we present the first results on the catalytic activity of pre-formed metal nanoparticles adsorbed at the liquid–liquid interface. This is an ideal system to probe catalytic properties of metal nanomaterials without a solid substrate, which can affect electrocatalytic properties by perturbing the electrochemical double layer. In addition, this setup permits the catalytic properties of metals to be combined with the unique possibilities of the liquid–liquid setup, given that a three phase boundary is formed, such as higher solubilities of reactants (or products) in the organic solvents. New electrocatalytic reactions may, therefore, emerge from the study of catalytic process at the ITIES.

## Acknowledgements

We thank the EPSRC (grant references EP/H047786/1 and EP/K007025/1) for funding.

## References

[1] I. Hatay, B. Su, F. Li, M.A. Mendez, T. Khoury, C.P. Gros, J.-M. Barbe, M. Ersoz, Z. Samec, H.H. Girault, Proton-coupled oxygen reduction at liquid–liquid interfaces catalyzed by cobalt porphine, Journal of the American Chemical Society 131 (2009) 13453.
[2] M.A. Mendez, R. Partovi-Nia, I. Hatay, B. Su, P.Y. Ge, A.J. Olaya, N. Younan, M. Hojeij, H.H. Girault, Molecular electrocatalysis at soft interfaces, Physical Chemistry Chemical Physics 12 (2010) 15132.
[3] A.J. Olaya, D. Schaming, P.-F. Brevet, H. Nagatani, T. Zimmermann, J. Vanicek, H.-J. Xu, C.P. Gros, J.-M. Barbe, H.H. Girault, Self-assembled molecular rafts at liquid|liquid interfaces for four-electron oxygen reduction, Journal of the American Chemical Society 134 (2012) 498.
[4] B. Su, I. Hatay, A. Trojanek, Z. Samec, T. Khoury, C.P. Gros, J.-M. Barbe, A. Daina, P.-A. Carrupt, H.H. Girault, Molecular electrocatalysis for oxygen reduction by cobalt porphyrins adsorbed at liquid/liquid interfaces, Journal of the American Chemical Society 132 (2010) 2655.
[5] J.J. Nieminen, I. Hatay, P.Y. Ge, M.A. Mendez, L. Murtomaki, H.H. Girault, Hydrogen evolution catalyzed by electrodeposited nanoparticles at the liquid|liquid interface, Chemical Communications 47 (2011) 5548.
[6] C. Johans, R. Lahtinen, K. Kontturi, D.J. Schiffrin, Nucleation at liquid|liquid interfaces: electrodeposition without electrodes, Journal of Electroanalytical Chemistry 488 (2000) 99.
[7] P. Ge, M.D. Scanlon, P. Peljo, X. Bian, H. Vrubel, A. O'Neill, J.N. Coleman, M. Cantoni, X. Hu, K. Kontturi, B. Liu, H.H. Girault, Hydrogen evolution across nano-Schottky junctions at carbon supported catalysts in biphasic liquid systems, Chemical Communications 48 (2012) 6484.
[8] I. Hatay, P.Y. Ge, H. Vrubel, X. Hu, H.H. Girault, Hydrogen evolution at polarised liquid/liquid interfaces catalyzed by molybdenum disulfide, Energy and Environmental Science 4 (2011) 4246.
[9] I. Hatay, B. Su, F. Li, R. Partovi-Nia, H. Vrubel, X. Hu, M. Ersoz, H.H. Girault, Hydrogen evolution at liquid–liquid interfaces, Angewandte Chemie International Edition 48 (2009) 5139.
[10] P. Peljo, T. Rauhala, L. Murtomaki, T. Kallio, K. Kontturi, Oxygen reduction at a awater-1,2-dichlorobenzene interface catalyzed by cobalt tetraphenyl porphyrine – a fuel cell approach, International Journal of Hydrogen Energy 36 (2011) 10033.
[11] B. Su, R. Partovi-Nia, F. Li, M. Hojeij, M. Prudent, C. Cominboeuf, Z. Samec, H.H. Girault, $H_2O_2$ generation by cecamethylferrocene at a liquid|liquid interface, Angewandte Chemie International Edition 47 (2008) 4675.
[12] F. Li, F. Cortes-Salazar, R. Partovi-Nia, H.H. Girault, Detection of hydrogen peroxide at a liquid/liquid interface using scanning electrochemical microscopy, Electrochemistry Communications 11 (2009) 473.
[13] A. Trojanek, J. Langmaier, B. Su, H.H. Girault, Z. Samec, Electrochemical evidence of catalysis of oxygen reduction at polarized liquid–liquid interface by tetraphenylporhphyrin monoacid and diacid, Electrochemistry Communications 11 (2009) 1940.
[14] M. Hojeij, N. Younan, L. Ribeaucourt, H.H. Girault, Surface plasmon resonance of gold nanoparticles assemblies at liqui|liquid interfaces, Nanoscale 2 (2010) 1665.
[15] A.A. Kornyshev, M. Marinescu, J. Paget, M. Urbakh, Reflection of light by metal nanoparticles at electrodes, Physical Chemistry Chemical Physics 14 (2012) 1850.
[16] N. Younan, M. Hojeij, L. Ribeaucourt, H.H. Girault, Electrochemical properties of gold nanoparticles assembly at polarised liquid|liquid interfaces, Electrochemistry Communications 12 (2010) 912.
[17] M. Marinescu, M. Urbakh, A.A. Kornyshev, Voltage dependent capacitance of metallic nanoparticles at a liquid/liquid interface, Physical Chemistry Chemical Physics 14 (2012) 1371.
[18] D. Schaming, M. Hojeij, N. Younan, H. Nagatani, H.J. Lee, H.H. Girault, Photocurrents at polarized liquid|liqudi interfaces enhanced by gold nanoparticle film, Physical Chemistry Chemical Physics 13 (2011) 17704.
[19] T. Brulle, W. Ju, P. Niedermayr, A. Denisenko, O. Paschos, O. Schneider, U. Stimming, Size-dependent electrocatalysis activity of gold nanoparticles on HOPG and highly boron doped diamond surfaces, Molecules 16 (2011) 10059.
[20] T. Inasaki, S. Kobayashi, Particle size effects of gold on the kinetics of the oxygen reduction at chemically prepared Au/C catalysts, Electrochimica Acta 54 (2009) 4893.
[21] M.G. Mones de Oca, D. Plana, V. Celorrio, M.J. Lazaro, D.J. Fermin, Electrocatalytic properties of strained Pd nanoshells at Au nanostructures: CO, HCOOH oxidation, Journal of Physical Chemistry C 116 (2011) 692.
[22] M.S. El-Deab, T. Ohsaka, Hydrodynamic voltammetric studies of the oxygen reduction at gold nanoparticles-electrodeposited gold electrodes, Electrochimica Acta 47 (2002) 4255.
[23] F. Mirkhalaf, K. Tammeveski, D.J. Schiffrin, Electrochemical reduction of oxygen on nanoparticulate gold electrodeposited on a molecular template, Physical Chemistry Chemical Physics 11 (2009) 3463.
[24] V. Celorrio, M.G. Montes de Oca, D. Plana, R. Moliner, D.J. Fermin, M.J. Lazaro, Electrochemical performance of Pd and Au–Pd core–shell nanoparticles on surface tailored carbon black as catalyst support, International Journal of Hydrogen Energy 37 (2012) 7152.
[25] J. Jirkovsky, M. Halasa, D.J. Schiffrin, Kinetics of electrocatalytic reduction of oxygen and hydrogen peroxide on dispersed gold nanoparticles, Physical Chemistry Chemical Physics 12 (2010) 8042.
[26] H. Hotta, N. Akagi, T. Sugihara, S. Ichikawa, T. Osakai, Electron-conductor separating oil-water (ECSOW) system: a new strategy for characterizing electron-transfer processes at the oil/water interface, Electrochemistry Communications 4 (2002) 472.
[27] J. Turkevich, P.C. Stevenson, J. Hillier, A study of the nucleation and growth processes in the synthesis of colloidal gold, Faraday Discussions 11 (1951) 75.
[28] M.G. Montes de Oca, H. Kumarakura, D. Cherns, D.J. Fermin, Article hydrogen adsorption at strained Pd nanoshells, Journal of Physical Chemistry C 115 (2010) 10489.
[29] G. Frens, Controlled nucleation for the regulation of the particle size in monodisperse gold suspensions, Nature Physical Science 241 (1973) 20.
[30] J.W. Hu, Y. Zhang, J.-F. Li, Z. Liu, B. Ren, S.-G. Sun, Z.-Q. Tian, T. Lian, Synthesis of Au@Pd core–shell nanoparticles with controllable size and their application in surface-enhanced Raman spectroscopy, Chemical Physics Letters 408 (2005) 354.
[31] G. Schmid, A. Lehnert, J.O. Malm, J.O. Bovin, You have full text access to this content ligand-stabilized bimetallic colloids identified by HRTEM and EDX (pages 874–876), Angewandte Chemie International Edition 30 (1991) 874.
[32] N. Laanait, J. Yoon, B. Hou, P. Vanysek, M. Meron, B. Lin, G. Luo, M.L. Schlossman, Monovalent ion condensation at the electrified liquid/liquid interface, Journal of Chemical Physics 132 (2010) 171101.
[33] A. Sabela, V. Marecek, Z. Samec, R. Fuoco, Standard Gibbs energies of transfer of univalent ions from water to 1,2-dichloroethane, Electrochimica Acta 37 (1992) 231.
[34] Y. Shao, A.A. Stewart, H.H. Girault, Determination of the half-wave potential of the species limiting the potential window. Measurement of gibbs transfer energies at the water/1,2-dichloroethane interface, Journal of the Chemical Society, Faraday Transactions 87 (1991) 2593.
[35] B. Hundhammer, C. Muller, SolomonT., H. Alemu, H. Hassan, In transfer across water-o-dichlorobenzene interface, Journal of Electroanalytical Chemistry 319 (1991) 125.
[36] B. Su, J.-P. Abid, D.J. Fermin, H.H. Girault, H. Hoffmannova, P. Krtil, Z. Samec, Reversible voltage-induced assembly of Au nanoparticles at liquid|liquid interfaces, Journal of the American Chemical Society 126 (2003) 915.
[37] H. Jensen, D.J. Fermin, J.E. Moser, H.H. Girault, Organization, Reactivity of nanoparticles at molecular interfaces. Part I. Photoelectrochemical responses involving $TiO_2$ nanoparticles assembled at polarizable water|1,2-dichloroethane junctions, Journal of Physical Chemistry B 106 (2002) 10909.
[38] Z. Samec, Electrochemistry at the interface between two immiscible electrolyte solutions, Pure and Applied Chemistry 76 (2004) 2147.
[39] M. Brust, G.J. Gordillo, Electrocatalytic hydrogen redox chemistry on gold nanoparticles, Journal of the American Chemical Society 134 (2012) 3318.
[40] S. Biggs, P. Mulvaney, C.F. Zukoski, F. Grieser, Study of anion adsorption at the gold-aqueous solution interface by atomic force microscopy, Journal of the American Chemical Society 116 (1994) 9150.
[41] J. Kunze, I. Burgess, R.J. Nichols, C. Buess-Herman, J. Lipkowski, Electrochemical evaluation of citrate adsorption on Au(1 1 1) and the stability of citrate reduced gold colloids, Journal of Electroanalytical Chemistry 599 (2007) 147.
[42] Z. Shi, J. Lipkowski, Chloride adsorption at the Au(1 1 1) electrode surface, Journal of Electroanalytical Chemistry 403 (1996) 225.
[43] O.M. Magnussen, Ordered anion adlayers on metal electrode surfaces, Chemical Reviews 102 (2002) 679.
[44] D. Eberhardt, E. Santos, W. Schmickler, Impedance studies of reconstructed and non-reconstructed gold single crystal-surfaces, Journal of Electroanalytical Chemistry 419 (1996) 23.